Vision-based kinematic calibration of a H4 parallel mechanism

Pierre Renaud, Nicolas Andreff, Frédéric Marquet, Philippe Martinet

Vision-based kinematic calibration of a H4 parallel mechanism

Pierre Renaud [1], Nicolas Andreff [1], Frédéric Marquet [2], Philippe Martinet [3]

[1]LaRAMA, U. Blaise Pascal/IFMA, Clermont-Ferrand, France, renaud/andreff@ifma.fr
[2]LIRMM, U. Montpellier II/CNRS, Montpellier, France, marquet@lirmm.fr
[3]LASMEA, U. Blaise Pascal/CNRS, Clermont-Ferrand, France, martinet@lasmea.univ-bpclermont.fr

Abstract - In this article, we present the kinematic calibration of a H4 parallel robot using a vision-based measuring device. Calibration is performed according to the inverse kinematic model method, using first the design model then a model developed for calibration purpose. With a precision of the order of magnitude of 0.2mm and 0.03°, our vision system allowed us to obtain a final positioning accuracy of the end-effector lower than 0.5mm. Conclusions are given on the use of a vision-based measuring device for the calibration of this class of mechanisms.

I. INTRODUCTION

Compared to serial mechanisms, parallel structures may exhibit a much better repeatability [1], but their large number of links and passive joints often limits their performance in terms of accuracy [2]. A kinematic calibration is thus needed. The algorithms proposed to conduct calibration for parallel structures can be classified in three classes: methods based on the direct use of a kinematic model, on the use of kinematic constraints on mechanism parts, and methods relying on the use of redundant proprioceptive sensors.

The use of additional proprioceptive sensors on the passive joints of the mechanism enables one to have a unique solution to the direct kinematic model [3], and to perform the kinematic calibration [4, 5, 6], or to improve their accuracy [7]. Practically speaking, the mechanism design has to take into account the use of such extra sensors. Nevertheless, not all kinds of mechanisms can be equipped with additional sensors.

Methods based on kinematic constraints of the end-effector [6] or the legs [8, 9, 10, 11] solve this problem. However, the former methods are not numerically efficient [6], and kinematic constraints of the legs of the mechanism in position or orientation seem difficult to achieve in practice on large structures.

The forward kinematic model of parallel structures can rarely be expressed analytically [1]. The use of this model to achieve kinematic calibration may consequently lead to numerical instability [6]. On the other hand, the inverse kinematic model can usually easily be derived. Calibration can then be performed by comparing the measured joint variables and their corresponding values estimated from the measured end-effector pose and the inverse kinematic model. Each leg can furthermore be calibrated independently [12]. Up to now, the inverse kinematic model method seems the most efficient method [6].

Its main limitation is the need for accurate measurement of the full end-effector pose (*i.e.* both its position and its orientation). Among the proposed measuring devices [13, 14, 15, 16], only a few have been used to conduct kinematic identification of a parallel structure [12, 17, 18, 19]. Indeed, the systems are either very expensive, tedious to use or with low working volume. On the opposite, a vision-based measuring system enables one to perform the pose measurement accurately [20], is low-cost and easy to use. Using this device and the inverse kinematic method may therefore be an efficient way to conduct kinematic calibration.

In this article, we present the kinematic calibration of a H4 robot [21] using a vision-based measuring device. In the first part, two different kinematic models are detailed. The first one (Model 12) corresponds to the initial design of the mechanism, and the second one (Model 31) is developed for calibration purpose. The use of a vision-based measuring system for kinematic calibration is then analyzed. The identifiability conditions bound to the use of such an exteroceptive sensor are underlined. Experimental results on a H4 prototype are then presented with validation experiments, showing a final positioning accuracy of the end-effector of less than 0.5mm. The calibration gain induced by the use of the calibration model is discussed. Finally conclusions are given on the use of a vision-based measuring device for the calibration of this class of mechanisms.

II. KINEMATIC MODELLING

A. H4 Description

The H4 mechanism (Fig. 1) is a parallel mechanism composed of four chains, actuated by four angular motors located between the base and the arms. The forearms
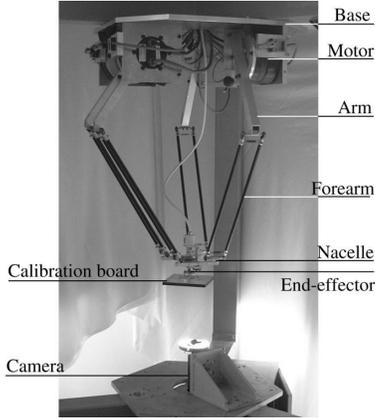
Fig. 1 : H4 and vision-based measuring system

Fig. 2 : Location of the joints between base and forearms
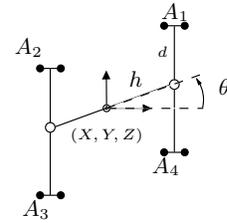
Fig. 3 : Definition of the nacelle's angle

linking the arms and the nacelle are composed of two rods. The end-effector has four degrees of freedom (three translations and one rotation) if the closed loops constituted by these four pairs of rods correspond to spatial parallelograms [21]. The end-effector is linked to the nacelle with a mechanical amplification system to achieve a higher rotation capability.

B. Model 12

Hypotheses. In the following, the end-effector will be assumed to have only four degrees of freedom. The hypothesis validity will be discussed in paragraph IV. Each forearm parallelogram is assumed perfect and is thus equivalent to a link ensuring a circular translation of the nacelle with respect to the arm. In this part, we assume furthermore that the rotary joint centers $P_i, i \in [1, 4]$ between the base and the arms are located in the same plane, at equal distance R from the corresponding joint centers A_i on the nacelle when this latter is considered to be in the base plane (Fig. 2). The four arms are supposed to be of equal length L, and the forearms of length l. Considering the nacelle dimensions h and d (Fig. 3), the mechanism geometry is therefore defined by nine parameters : R, l, L, h, d, α_i with $i \in [1, 4]$. With such a model, parameter d has however no influence on the kinematics [21]. Taking into account the joint offsets q_{i_0}, $i \in [1, 4]$, twelve parameters finally define the mechanism kinematics.

Inverse Kinematic Model. An implicit model can be readily written between end-effector pose (X, Y, Z, θ) (Fig. 3) and joint variables by expressing the i-th forearm length, $i \in [1, 4]$ as a function of the parameters [21]:

$$L^2 - l^2 - \|\overrightarrow{P_iA_i}\|^2 = -2 \begin{pmatrix} \overrightarrow{P_iA_i}_x.l.cos(\alpha_i).cos(q_i) \\ +\overrightarrow{P_iA_i}_y.l.sin(\alpha_i).cos(q_i) \\ -\overrightarrow{P_iA_i}_z.l.sin(q_i) \end{pmatrix} \quad (1)$$

The inverse kinematic model can then be derived from this implicit model [21]:

$$q_i = 2.Atan\left(\frac{N + \epsilon_i\sqrt{N^2 + M^2 - G^2}}{G + M}\right), i \in [1, 4] \quad (2)$$

with $G = L^2 - l^2 - \|\overrightarrow{P_iA_i}\|^2$, $N = 2.l.\overrightarrow{P_iA_i}_z$
$M = -2.l.(\overrightarrow{P_iA_i}_x.cos(\alpha_i) + \overrightarrow{P_iA_i}_y.sin(\alpha_i))$ and $\epsilon_i = \pm 1$ depending on the assembly

Calibration method. To identify the parameter vector ξ, an error function is minimized, which compares the estimated joint variables and the measured ones $\tilde{q}$ for N different end-effector poses $(X_j, Y_j, Z_j, \theta_j)$:

$$\min_\xi \sum_{j=1}^{N} \sum_{i=1}^{4} \left(q_i(\xi, X_j, Y_j, Z_j, \theta_j) - \tilde{q}_{ij}\right)^2 \quad (3)$$

C. Model 31

Hypotheses. The former geometry corresponds to the mechanism design. Due to the manufacturing tolerances, assembly errors, the previous assumptions about the geometry may be questionable. In this part, the mechanism is still considered as a four degrees of freedom mechanism and the nacelle is assumed to be planar with dimensions h et d. On the other hand, no assumption is now made about the position and orientation of the revolute joints

TABLE 1 : Model 31 kinematic parameters

| Designation	Parameter
x_i, y_i, z_i, $i \in [2, 4]$	Rotary joint positions
ψ_i, β_i, $i \in [1, 4]$	Rotary joint orientations
q_{i_0}, $i \in [1, 4]$	Joint offsets
l_i, L_i, $i \in [1, 4]$	Arm and forearm lengths
h, d	Nacelle dimensions
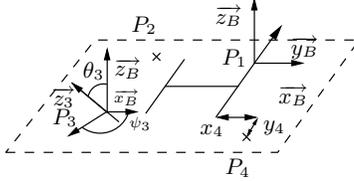
Fig. 4 : Definition of the base frame and orientation of rotary joint between base and arm for the Model 31

between the base and the arms, nor on the arm and forearm lengths.

The base frame is attached to the first joint center P_1 (Fig. 4), its axis $\overrightarrow{z_B}$ parallel to the end-effector rotation axis, and orientation defined by the "H-configuration" of the nacelle. The position of the joint centers P_i is defined relatively to the corresponding joint centers on the nacelle in a similar way to the Model 12. The joint axis $\overrightarrow{z_i}$ are defined by Euler angles ψ_i and β_i. Thirty-one parameters are then necessary to define its geometry (Table 1).

Implicit model. The implicit model can be obtained as in II.B. for each kinematic chain $i \in [1, 4]$:

$$\|L_i\overrightarrow{V_i} + \overrightarrow{W_i}\|^2 = l_i^2 \tag{4}$$

with
$$\overrightarrow{V_i} = \begin{pmatrix} sin(q_i+q_{i_0})cos(\beta_i)sin(\psi_i)-cos(q_i+q_{i_0})cos(\psi_i) \\ -sin(q_i+q_{i_0})cos(\beta_i)cos(\psi_i)-cos(q_i+q_{i_0})sin(\psi_i) \\ -sin(q_i+q_{i_0})sin(\beta_i) \end{pmatrix}$$
$$\overrightarrow{W_i} = \begin{pmatrix} X-x_i+(1+\epsilon_{1i}-\epsilon_{2i}cos(\theta))h \\ Y-y_i+d-\epsilon_{2i}hsin(\theta) \\ Z-z_i \end{pmatrix}$$

and $\epsilon_{1i} = \pm 1$, $\epsilon_{2i} = \pm 1$ depending on the assembly. The inverse kinematic model consists in expressing q_i as a function of (X, Y, Z, θ), which seems not possible analytically.

Calibration method. The parameter vector ξ is obtained from the implicit model by solving:

$$\min_\xi \sum_{j=1}^N \sum_{i=1}^4 \left(l_i - \|L_i\overrightarrow{V_{ij}} + \overrightarrow{W_{ij}}\| \right)^2 \tag{5}$$

III. FROM VISION TO CALIBRATION

In this part, we consider how to use vision to perform the kinematic calibration of the H4 mechanism.

A. Vision-based measurement characteristics

The vision-based measuring system is composed of a camera, fixed onto the base, and a calibration board fixed onto the end-effector (Fig. 1). The system is calibrated at the beginning of the experiment by acquiring a sequence of about 8 images, using a software developed at LASMEA [22]. After calibration, the pose $^C T_{cb}$ of the calibration board with respect to the camera can be computed for each image [23]. Furthermore, the measuring system is easy to use, and the experimental procedure for the kinematic calibration is fast.

The full-pose measurement enables one to perform calibration by the inverse kinematic model method. In this model, the end-effector pose $^B T_{ee}$ is defined by its position and orientation with respect to the base frame, and related to the pose measurement by the relation:

$$^B T_{ee} = {}^B T_C {}^C T_{cb} {}^{cb} T_{ee} \tag{6}$$

Two transformations have therefore to be identified simultaneously with the kinematic parameters: $^B T_C$ between the camera and base frames, and $^{cb} T_{ee}$ between the calibration board and the end-effector.

B. Prior Kinematic Analysis

Information about the kinematics of the system can be obtained before conducting the identification process. Indeed, the H4 robot has a constant rotation axis, perpendicular to the nacelle, provided that the assumption concerning the forearm parallelograms is valid. Consequently, the calibration board also rotates around this constant axis. The latter can hence be immediately estimated in the camera frame since the rotation matrix between the calibration board and the camera $^C R_{cb}$ can be computed for each end-effector pose. Furthermore, as the rotation axis corresponds to the vector $\overrightarrow{z_b}$, this vector can be identified in the camera frame R_C. This enables us to reduce the number of kinematic parameters identified simultaneously.

C. Identifiability

Model 12. Identifying $^C T_B$ and $^{cb} T_{ee}$ is equivalent to base-world and tool-hand calibration problems. Since the calibration board movement is limited to one rotation w.r.t the camera, the transformation $^{cb} T_{ee}$ cannot be completely identified [24, 25]. Moreover, in our context, due to visibility condition of the calibration board, the camera and calibration board are approximately aligned with

the mechanism rotation axis (Fig. 1). Then expanding (6) shows that $z_{cb,ee}$ and $z_{B,C}$ (the translation components along z of the transformations $^{cb}T_{ee}$ and $^{C}T_{B}$) can be identified only by their sum. Finally, as the angles defining parallelism between the end-effector and the calibration board have only a second-order influence, their identification seems also tedious. Hence the *a priori* value of these parameters will then be used. These remarks have been confirmed by the numerical estimation of the Jacobian matrix.

Model 31. This model is also invariant with respect to a simultaneous rotation of the location of the joints between the base and the legs, the camera frame and the calibration board frame around the axis $\overrightarrow{z_B}$. Therefore, one parameter between the two corresponding angles of the transformations $^{B}T_{C}$ and $^{cb}T_{ee}$ has here again to be fixed to its *a priori* value. In the same way, the nacelle dimension d and the translation component $y_{B,C}$ of the transformation $^{B}T_{C}$ are only identifiable by their sum. The *a priori* value of the parameter d is then used.

The identification by the inverse kinematic model method is therefore submitted to two identifiability problems: The first one is the number of degrees of freedom of the mechanism, that prevents from achieving the complete calibration of the transformations related to the measuring device. The second one comes from the number of degrees of freedom introduced in the joint location parameterization for the Model 31. We can also remark that the identification of the transformations related to the measuring device imply a global identification of the mechanism, and not the independent identification of each kinematic chain.

IV. EXPERIMENTATION

A. Set-up

The camera sensor has a resolution of 1024×768 pixels, $8bit$ encoded, with a 3.8 mm lens. Images are stored on a PC via an IEEE1394 bus. For each position, 10 images are stored and their average value is considered for the pose evaluation, in order to reduce high frequency noise. The pose can be measured with accuracy in the order of respectively 0.2 mm and 0.03° for each translation and rotation component.
Eighty-one poses are used, equally distributed in a $200 \times 200 \times 150$ mm^3 volume, with three different orientations ($\theta = -20°$, $0°$, $20°$). Out of them, seventy-one poses are randomly chosen for the calibration, the other ten are used to perform a validation test.

B. Kinematic Analysis

The variation of the rotation axis in the camera frame is quantified by the variation of the angle between the axis

TABLE 2 : *A priori* and identified kinematic parameters of the model 12 (IS units)

	h	l	R	L
a priori	0.060	0.2600	0.1400	0.4800
Identified	0.0610	0.2600	0.1413	0.4876
	α_1	α_2	α_3	α_4
a priori	0	3.1416	4.7124	4.7124
Identified	-0.0015	3.1016	4.6807	4.6859
	q_{0_1}	q_{0_2}	q_{0_3}	q_{0_4}
a priori	0	0	0	0
Identified	-0.0662	-0.0080	-0.0476	-0.0561

and its mean direction. The estimated standard deviation is equal to 0.12°. The amplitude of the axis direction variation confirms that the mechanism can be safely considered as having four degrees of freedom.

C. Identification

Model 12. The computation of the estimated parameters is achieved using the inverse kinematic model method, with non-linear optimization. The Levenberg-Marquardt algorithm is used, and columns of the identification Jacobian matrix are scaled with extremal scaling value [26] to avoid biased estimation. The identified parameters related to the mechanism are listed in Table 2, and compared to their *a priori* values.

It is noticeable that using the *a priori* parameters, rather than the optimally estimated ones, yields an average positioning error of the nacelle of $26mm$ and $0.022rad$.

Model 31. The angle around $\overrightarrow{z_B}$ between the nacelle and the calibration board identified with the Model 12 is used to achieve the kinematic calibration with the second model. The *a priori* value of d is employed.

D. Validation

Joint residuals. For Model 12, a first validation consists in estimating with the identified inverse kinematic model the joint variables from the ten pose measurements that were not used for calibration, and compare these values to the recorded joint variables. The mean and root mean square errors of the four joints are indicated in Table 3, showing an accuracy increase from some $0.1rad$ before calibration to some $10^{-4}rad$ afterwards. For Model 31, the validation is achieved by computing the errors committed in the joint variables estimation, to enable comparison with Model 12. The errors are of the same order.

Straightness evaluation. To confirm these results independently from the measuring device, an experiment is

TABLE 3 : Mean and root mean square errors on joint variables (rad)

Variable	q_1	q_2	q_3	q_4
Before calibration				
Mean	9.0^{E-2}	3.5^{E-2}	7.3^{E-2}	8.3^{E-2}
R.M.S	9.0^{E-2}	3.7^{E-2}	7.4^{E-2}	8.3^{E-2}
After calibration - Model 12				
Mean	7.1^{E-5}	1.1^{E-4}	-7.7^{E-4}	-2.1^{E-4}
R.M.S	1.4^{E-3}	1.3^{E-3}	1.4^{E-3}	2.6^{E-3}
After calibration - Model 31				
Mean	-2.0^{E-4}	5.2^{E-4}	-4.7^{E-4}	7.4^{E-5}
R.M.S	2.9^{E-3}	2.6^{E-3}	1.8^{E-3}	3.1^{E-3}

TABLE 4 : Straightness evaluation for the two experiments with initial and calibrated kinematic parameters

Direction	1	2
Before calib.	1.3^{E-3}	2.3^{E-3}
Model 12	4.9^{E-4}	5.8^{E-4}
Calib. model	5.9^{E-4}	1.1^{E-3}

conducted where the end-effector is manually constrained to follow a line materialized by a ruler (Fig. 5). The corresponding joint variables are stored. From these joint variables values, poses are computed by means of a numerical forward kinematic model. The physical set-up implies that these poses should lie on a straight line. Hence, the straightness of the line is computed for the two kinematic parameter sets (*a priori* and identified) as the root mean square of the distance between the different positions and the line estimated by a least squares criterion. The experiment is conducted with two different orientations of the rule. The results are presented in Table 4. For Model 12, the straightness improvement is equal to 63% and 75% , which confirms the first validation. For Model 31, the improvement is actually lower, with a relative gain around 50% for the two experiments. The low decrease of straightness improvement can be due to several factors. The first one is the diminution of the ratio between the pose number and the kinematic parameter number, even if this ratio remains acceptable (36 parameters and 284 equations). The second factor is the identifiability problem bound to the use of an exteroceptive measuring device. Eventually the hypothesis concerning the spatial parallelograms may be questionable, and a kinematic model taking into account the geometry of the rods may be necessary.

With the control law. Another validation is performed by introducing the identified kinematic parameters in the control law, which uses Model 12. The end-effector

Fig. 5 : Validation experiment - Kinematic constraint on the end-effector

is then displaced along a $100mm \times 100mm$ square trajectory, visualized graphically. The error committed on the square side is reduced from $5mm$ to less than $0.5mm$.

V. CONCLUSIONS

In this article, the kinematic calibration of a H4 parallel mechanism using a vision-based measuring device was presented. Using our vision system, a final positioning accuracy of the end-effector lower than $0.5mm$ could be obtained, and the accuracy improvement has been confirmed by several validation experiments. The vision-based measuring device allows us also to qualify directly the assumption validity concerning the number of degrees of freedom. For such a mechanism with less than six degrees of freedom, the parameter identifiability has been analyzed, showing that all the parameters related to the sensor installation cannot be identified.
The lower results with the second presented kinematic model need further analysis concerning the modelling of the spatial parallelograms. To get more information about the kinematics of the mechanism, the use of the camera to look at the legs of the mechanism will be also further investigated.

VI. ACKNOWLEDGEMENTS

References

[1] J.P. Merlet, *Les Robots Parallèles*, Hermès, Paris, 1997.

[2] J. Wang and O. Masory, "On the accuracy of a Stewart platform - Part I : The effect of manufacturing tolerances," in *Proc. of ICRA93*, 1993, pp. 114–120.

[3] L. Tancredi, M. Teillaud, and J.-P. Merlet, "Forward kinematics of a parallel manipulator with additional rotary sensors measuring the position of platform joints," in *Computational Kinematics*, J.-P. Merlet and B. Ravani, Eds., Dordrecht, 1995, pp. 261–270.

[4] C. Wampler and T. Arai, "Calibration of robots having kinematic closed loops using non-linear least-squares estimation," in *IFToMM*, Nagoya, September 1992, pp. 153–158.

[5] H. Zhuang, "Self-calibration of parallel mechanisms with a case study on Stewart platforms," *IEEE Trans. on Robotics and Automation*, vol. 13, no. 3, pp. 387–397, 1997.

[6] D. Daney, *Etalonnage géométrique des robots parallèles*, Ph.D. thesis, Université de Nice - Sophia Antipolis, 2000.

[7] F. Marquet, O. Company, S. Krut, and F. Pierrot, "Enhancing parallel robots accuracy with redundant sensors," in *Proc. of ICRA02*, Washington, May 2002, pp. 4114–4119.

[8] Z. Geng and L.S. Haynes, "An effective kinematics calibration method for Stewart platform," in *Proc. of Fifth International Symposium on Robotics and Manufacturing*, Hawaï, 1994, pp. 87–92.

[9] H. Zhuang and Z.S. Roth, "Method for kinematic calibration of Stewart platforms," *J. of Robotic Systems*, vol. 10, no. 3, pp. 391–405, 1993.

[10] W. Khalil and S. Besnard, "Self calibration of Stewart-Gough parallel robots without extra sensors," *IEEE Trans. on Robotics and Automation*, pp. 1758–1763, 1999.

[11] D. Daney, "Self calibration of Gough platform using leg mobility constraints," in *Proc of the 10th world congress on the theory of machine and mechanisms*, 1999, pp. 104–109.

[12] H. Zhuang, J. Yan, and O. Masory, "Calibration of Stewart platforms and other parallel manipulators by minimizing inverse kinematic residuals," *J. of Robotic Systems*, vol. 15, no. 7, pp. 395–405, 1998.

[13] J.F. Curtino, D.E. Schinstock, and M.J. Prather, "Three-dimensional metrology frame for precision applications," *Precision Engineering*, vol. 23, pp. 103–112, 1999.

[14] M. Vincze, J.P. Prenninger, and H. Gander, "A laser tracking system to measure position and orientation of robot end-effectors under motion," *Int. J. Robotics Research*, vol. 13, no. 4, pp. 305–314, 1994.

[15] O. Masory and Y. Jiahua, "Measurement of pose repeatability of Stewart platform," *J. of Robotic Systems*, vol. 12, no. 12, pp. 821–832, 1995.

[16] T. Schmitz and J. Zlegert, "A new sensor for the micrometre-level measurement of three-dimensional, dynamic contours," *Measurement Science Technology*, vol. 10, pp. 51–62, 1999.

[17] Z.J. Geng and L.S. Haynes, "A "3-2-1" kinematic configuration of a Stewart platform and its application to six degrees of freedom pose measurements," *Robotics and Computer-Integrated Manufacturing*, vol. 11, no. 1, pp. 23–34, 1994.

[18] G. Fried, K. Djouani, Y. Amirat, and C. François, "A 3-d sensor for parallel robot calibration. a parameter perturbation analysis," in *Recent Advances in Robot Kinematics*, 1996, pp. 451–460.

[19] P. Vischer and R. Clavel, "Kinematic calibration of the parallel delta robot," *Robotica*, vol. 16, pp. 207–218, 1998.

[20] P. Renaud, N. Andreff, M. Dhome, and P. Martinet, "Experimental evaluation of a vision-based measuring device for parallel machine-tool calibration," in *Proc. of IROS02*, Lausanne, October 2002, pp. 1868–1873.

[21] F. Pierrot, F. Marquet, O. Company, and T. Gil, "H4 parallel robot : Modeling, design and preliminary experiments," in *Proc. of ICRA01*, Seoul, Korea, 2001, pp. 3256–3261.

[22] JM. Lavest, M. Viala, and M. Dhome, "Do we really need an accurate calibration pattern to achieve a reliable camera calibration," in *Proceedings of ECCV98*, Freiburg, June 1998, pp. 158–174.

[23] M. Dhome, M. Richetin, J.T. Lapreste, and G. Rives, "Determination of the attitude of 3-D objects from a single perpsective view," *IEEE Trans. on Pattern Analysis and Machine Intelligence*, vol. 11, no. 12, pp. 1265–1278, 1989.

[24] R.Y. Tsai and R.K. Lenz, "A new technique for fully autonomous and efficient 3D robotics hand/eye calibration," *IEEE Trans. on Robotics and Automation*, vol. 5, no. 3, pp. 345–358, 1989.

[25] N. Andreff, R. Horaud, and B. Espiau, "Robot hand-eye calibration using structure-from-motion," *Int. J. Robotics Research*, vol. 20, no. 3, pp. 228–248, 2001.

[26] K. Schroer, *Robot Calibration*, chapter Theory of kinematic modelling and numerical procedures for robot calibration, pp. 157–196, Chapman & Hall, 1993.